

## Integrated point and edge matching on poor textural images constrained by self-adaptive triangulations

Bo Wu<sup>a,\*</sup>, Yunsheng Zhang<sup>a,b,c</sup>, Qing Zhu<sup>b</sup>

<sup>a</sup>Department of Land Surveying & Geo-Informatics, The Hong Kong Polytechnic University, Hung Hom, Kowloon, Hong Kong

<sup>b</sup>State Key Laboratory of Information Engineering in Surveying Mapping and Remote Sensing, Wuhan University, P.O. Box C310, 129 LuoYu Road, Wuhan, Hubei 430079, PR China

<sup>c</sup>School of Geosciences and Info-Physics, Central South University, 932 South Road Lushan, Changsha, Hunan 410083, PR China

### ARTICLE INFO

#### Article history:

Received 19 April 2011

Received in revised form 18 December 2011

Accepted 19 December 2011

Available online 21 January 2012

#### Keywords:

Image matching

Point matching

Edge matching

Triangle constraint

Self-adaptive propagation

### ABSTRACT

This paper presents an innovative image matching method for reliable and dense image matching on poor textural images, which is the integrated point and edge matching based on the self-adaptive edge-constrained triangulations. Firstly, several seed points and seed edges are obtained on the stereo images, and they are used to construct a pair of initial edge-constrained triangulations on the images. Then, points and edges are matched based on the triangle constraint and other constraints. The newly matched points and edges are inserted into the triangulations and the constrained triangulations are updated dynamically along with the matching propagation. The final results will be the final edge-constrained triangulations generated from the successfully matched points and edges. Experiments using typical space-borne, airborne, and terrestrial images with poor textures revealed that the integrated point and edge matching method based on self-adaptive triangulations is able to produce dense and reliable matching results. Moreover, from the final matched points and edges, 3D points and edges preserving the physical boundaries of objects can be further derived based on photogrammetric techniques, which is ideal for further object modeling applications.

© 2011 International Society for Photogrammetry and Remote Sensing, Inc. (ISPRS). Published by Elsevier B.V. All rights reserved.

## 1. Introduction

Image matching is used for finding corresponding pixels in a pair of images, which allows 3D reconstruction by triangulation. It is also an essential and difficult task in digital photogrammetry and computer vision (Lhuillier and Quan, 2002; Hartley and Zisserman, 2003; Zhang and Gruen, 2006). Image matching is relatively easy when encountered with good image texture conditions. However, on relatively poor textural images such as the examples given in Fig. 1, image matching is a difficult and challenging problem. Most of the traditional digital photogrammetry systems require lots of human interactions to remove the errors in the matching results when dealing with poor textural images (Heipke et al., 2007).

The poor textural images focused on in this paper mainly refer to those images (space-borne, airborne, and terrestrial images) with textural conditions that are difficult for image matching, such as images with few or homogeneous textures, image textures with low contrasts, image textures with repetitive patterns, and image textures suffering from surface discontinuity or occlusion

problems. Fig. 1 shows typical examples of images with poor textures. Fig. 1(a and b) is a stereo pair of Mars surface images acquired at crater Victoria, in Meridiani Planum, by the HiRISE (High Resolution Imaging Science Experiment) camera on board the Mars Reconnaissance Orbiter in 2006 (McEwen et al., 2007). The HiRISE imagery has a resolution of 0.3 m/pixel and provides a tremendous amount of information for Martian topographic mapping. However, the stereo HiRISE images at the Victoria crater were extremely unfavorable for automated image matching (Kirk et al., 2007), with extensive areas that are almost featureless, extremely steep, and similar textural patterns are distributed in the sand dunes in the crater bottom area as indicated in Fig. 1(a and b). Fig. 1(c and d) is a stereo pair of aerial imagery acquired in the highland area in Lanzhou, China. This area is full of layer patterns. Image matching may fail easily in these areas due to the repetitive textural patterns, homogeneous and low contrast textures in local image regions. Fig. 1(e and f) shows a stereo pair of terrestrial close-range images of a building, in which the repetitive patterns of the brick structure on the building wall and surface discontinuities (e.g., the left side of the regions inside the doors) bring significant matching ambiguities to image matching.

Reliable image matching received a lot of attention in the past (Lowe, 1999; Tao et al., 2001; Lhuillier and Quan, 2002; Zhang

\* Corresponding author. Tel.: +852 2766 4335; fax: +852 2330 2994.

E-mail address: lsbowu@polyu.edu.hk (B. Wu).

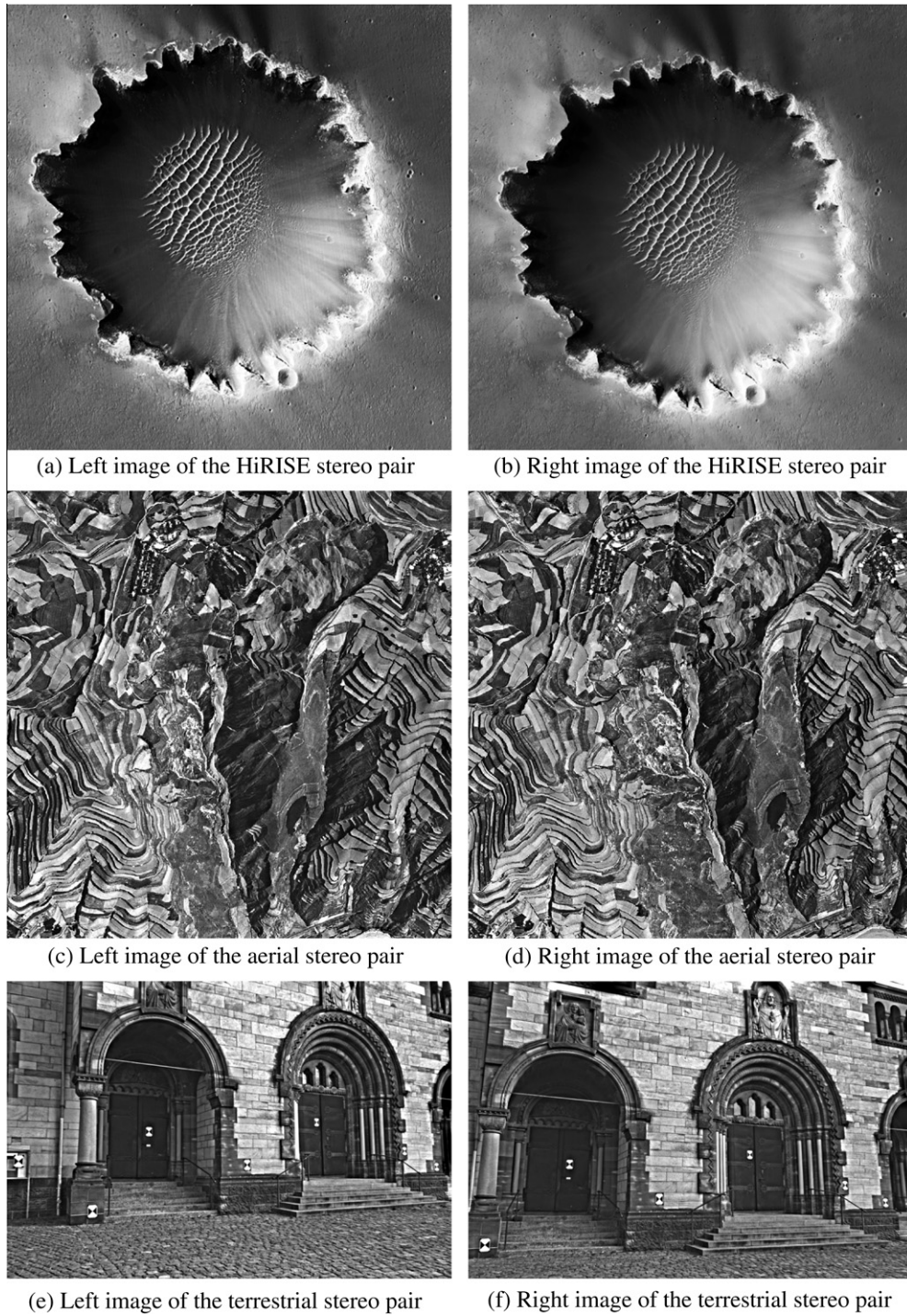


**Fig. 1.** Examples of stereo images with poor textures for image matching.

and Gruen, 2006; Furukawa and Ponce, 2010). Zhu et al. (2005, 2007a, 2010) presented an innovative image matching method, in which interest points are matched under the constraints of self-adaptive triangulations. The triangulations are dynamically updated along with the matching process by inserting the newly matched points into the triangulations. Because the most distinctive point is always successfully matched first, the dynamic updating of triangulations is just the process of self-adaptive matching propagation, which can adapt to the changes in image texture automatically and will finally produce more reliable matching results. This method has been used for stereo aerial image matching

(Zhu et al., 2005, 2007a; Wu, 2006) and close-range image matching (Wu et al., 2011; Zhu et al., 2010) and it proved able to produce reliable matching results. However, the existing methods only take account of point matching and its performance on poor textural images (as those illustrated in Fig. 1) is sometimes limited, which means only sparse matching points can be obtained to insure a favorable matching reliability. To improve the image matching performance on poor textural images, an instinctive idea will be incorporating edge features in an integrated point and edge matching propagation constrained by self-adaptive triangulations. From the examples of poor textural images in Fig. 1, one can

immediately notice that edge features can be used to segment the images, which will certainly be helpful to reduce matching ambiguities in the areas around the edges. This is particularly useful for the homogeneous or repetitive textural patterns (e.g., the sand dune area in Fig. 1(a), the layer structure in Fig. 1(c), and the brick wall in Fig. 1(e)) and areas with surface discontinuity problems (e.g., the crater rim area in Fig. 1(a) and the margin area of the door in Fig. 1(e)). Therefore, this paper presents an integrated point and edge matching method constrained by self-adaptive triangulations to improve the image matching performance on poor textural conditions based on our previous work (Zhu et al., 2005, 2007a; Wu, 2006; Wu et al., 2011).

After giving a literature review on image matching methods for poor textural images, an integrated point and edge matching method based on the self-adaptive triangle constraint is presented in detail. The stereo pairs of poor textural images illustrated in Fig. 1 are employed for experimental analysis and quantitative evaluation of the developed method. And finally, concluding remarks are presented and discussed.

## 2. Related work

Reliable and automatic image matching is a challenging task, especially for matching on poor textural images. One strategy is to use some complex descriptors to match the interest points detected on the images, of which SIFT (Scale Invariant Feature Transform) is the most well-known method (Lowe, 1999). SIFT combines a scale invariant interest point detector and a descriptor generated from the gradient distribution in the detected local regions. The SIFT method provides robustness against errors caused by image distortions from scale or orientation changes. However, it can only detect blob-like interest points and produce relative sparse matching results (Mikolajczyk and Schmid, 2004; Zhu et al., 2007b). Similar methods also include the SURF method presented by Bay et al. (2008) and the DAISY method by Tola et al. (2010). All these methods depend on complex descriptors and even though they may not work for the poor textural image sometimes.

Using redundant information (multiple images) to enhance image matching on poor textural conditions is another strategy. Zhang (2005) presented a multiple image matching method for DEM (Digital Elevation Model) generation using three-view aerial images. This method is based on a hypothesis that the surface constructed from the matched points should be relatively smooth in object space. The commercial software of Match-T (Match-T DSM, 2011) also provides functions of selecting stereo pairs to run stereo image matching; then merges the result of several matches to reduce the matching ambiguity by filtering them in 3D space. Seitz et al. (2006) performed a study to compare and evaluate multi-view stereo reconstruction algorithms. They concluded that matching with multiple images is useful for reducing matching ambiguity resulting from occlusions, surface discontinuities, and repetitive patterns or homogenous texture. However, multiple images are not always available.

The third strategy introduces segment constraints (edges or lines) into image matching. Tao et al. (2001) presented a matching method for images that lack texture involving segment constraints, which is based on an assumption that the disparity or depth in a segment shares the same plane fitting equation. This method may be invalid for a non-planar scene. Edge features are also helpful to model the surface discontinuity situations often seen on poor textural images. The Match-T software provides tools to measure break lines before image matching, which will then be used to constraint the subsequent image matching so as to obtain precise surface reconstruction results. Zhang et al.

(2007) presents a hybrid image matching approach, which takes the edges into consideration. Zhang and Gruen (2006) and Zhang and Fraser (2009) employed line feature as matching primitives and the matched lines are incorporated in the final DEM as break-lines. However, the edge or line features in these methods are only used as constraints. They are separated from the point matching. Their potential contributions to the image matching are not fully exploited.

The forth strategy to improve the matching reliability on poor textural images is to make use of certain matching propagation methods to inherit prior information from previous reliable matching results to enhance the later matching process. The traditional hierarchical matching methods based on image pyramid (Zhang and Gruen, 2006) or region growing methods (Otto and Chau, 1989; Lhuillier and Quan, 2002) are good examples. Zhu et al. (2005, 2007a, 2010) presented an image matching method based on the self-adaptive triangulations. The triangulations are dynamically updated along with the matching process by inserting the newly matched points into the triangulations. The dynamic updating of triangulations is adaptive to the image textures by propagating the matching from good textural areas to difficult areas. However, the current method only takes account of interest point matching, while the important edge features are not used. In previous work, the triangle constraint is sometimes invalid when there are edges (usually related to surface discontinuities) passing through the corresponding triangles, especially when the triangles cover a large area. Incorporating edge features in image matching is essential in these cases to further improve the matching performance, especially for poor textural images.

Based on the previous research (Zhu et al., 2005, 2007a; Wu, 2006; Wu et al., 2011), this paper presents an integrated point and edge matching method, which incorporates the edge matching with point matching in the same dynamic matching propagation process. This method takes advantage of the edge-constrained Delaunay triangulations with the capability of generating point and edge matches preserving the actual textural features. This strategy will be helpful to improve the image matching reliability, especially for poor textural images. The details are described in the following sections.

## 3. Integrated point and edge matching based on the self-adaptive triangulations

### 3.1. Overview of the approach

For a stereo pair of images, the method begins by extracting point and edge features on the images. A few seed points will be matched first from the extracted feature points. A few seed edges close to the successfully matched seed points will also be matched. They together will be used to generate a pair of initial edge-constrained corresponding triangulations on the stereo images. Then, an integrated point and edge matching propagation will be carried out, which includes two steps. The first is a feature to feature matching process for all the extracted point and edge features on the stereo images. The second step is a feature to area matching process, which will match the remaining point and edge features in one image after the first step with all the pixels in another image. The newly matched corresponding points and edges will be inserted into the triangulations and the triangulations will be updated dynamically along with the matching propagation. The final results will be the final edge-constrained corresponding triangulations generated from the successfully matched points and edges. The framework of the method is illustrated in Fig. 2.

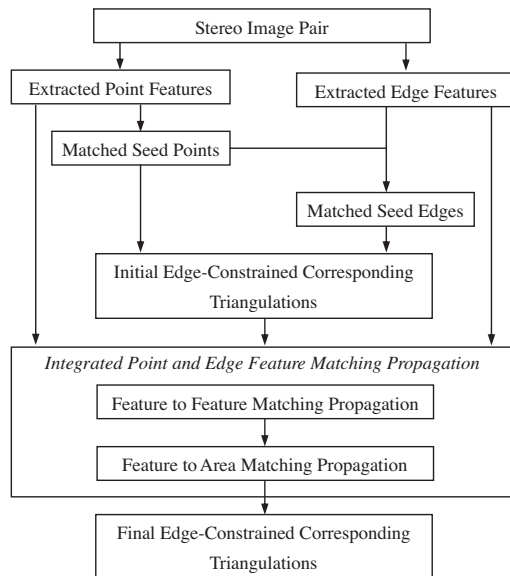


**Fig. 2.** The framework of the integrated point and edge matching method.

### 3.2. Point feature extraction and matching

#### 3.2.1. Point feature extraction

There are two types of interest point detectors used in this method. The first one is the SIFT for the purpose of selecting seed points. The SIFT algorithm (Lowe, 1999) is proved to be able to produce robust but relative sparse corresponding points invariant to moderate scale changes or distortions, which is ideal for the purpose of generating a small number of seed points on the poor textual images.

However, as mentioned in Section 2, the SIFT method only responds to blob-like points (Mikolajczyk and Schmid, 2004) and produces relative sparse corresponding points (Zhu et al., 2007b), while interesting points in highly textured areas such as the corners of roads or building boundaries may not be able to be derived by using SIFT method. This disadvantage limits its use in surface reconstruction in photogrammetry since dense and reliable matching results are critical for this task. Therefore, this paper uses another detector to extract interest points for the rest of the image matching, which is an improved Harris–Laplace method (Mikolajczyk and Schmid, 2004; Zhu et al., 2007b). This improved Harris–Laplace method responds to all types of interest points including corners and highly textured points and is also invariant to image scale and affine changes.

#### 3.2.2. Seed point matching

The interesting points detected using the SIFT method are used to match for a few seed points based on the SIFT descriptors. In the SIFT descriptor, each interest point is characterized by a vector with 128 unsigned eight-bit numbers generated from a local region, which defines the multi-scale gradient orientation histogram. The matching is performed by measuring the similarity between the two vectors associated with the two matching points (Lowe, 2004).

However, after the SIFT matching, mismatches may exist. Therefore, a RANSAC (Fischler and Bolles, 1981) approach is used to detect and remove possible mismatches from the previous SIFT matching results. The RANSAC algorithm starts by randomly selecting a portion of the matched corresponding points. A model is then built based on the fundamental matrix determined from the chosen matched points. This model is then used to determine

how much of the remaining corresponding points fit the model by determining whether each pair of corresponding points fit reasonably well to the model. This is used as a criterion to determine the best model which has the largest number of correct corresponding points. This process is repeated to find the overall best model. Those matched points that do not fit for the final best model are considered as mismatches and removed from the seed points. Details about using the SIFT method and RANSAC approach to obtain a few robust seed points can be found in Wu et al. (2011).

#### 3.2.3. Point matching based on the self-adaptive triangulations

Zhu et al. (2005, 2007a, 2010) presented an image matching method based on the self-adaptive triangulations. At first, a few pre-identified seed points are used to generate initial Delaunay triangulations. Then, interest points detected within a pair of triangles in the initial triangulations are matched under the triangle constraint, epipolar constraint, and disparity constraint. A left-right consistency check is incorporated in the matching process. After a pair of corresponding points with maximum reliability is obtained, they are inserted into the triangulations and the triangulations are updated immediately. Then, the next pair of triangles are handled, and the same process is repeated until the termination conditions (the triangles are small enough or cannot match successfully for at least one pair of points) of the matching propagation are met. As the most distinctive point is always successfully matched first, the dynamic updating of triangulations is adaptive to the image textures by propagating the matching from good textural areas to difficult areas. The geometry constraint of triangles can adapt to the changes in image texture automatically and will finally produce more reliable matching results. The same strategy is extended here for point feature matching on poor textural images by incorporating the edge-constrained triangulations. Details about the point matching method based on the self-adaptive triangulations can be found in Zhu et al. (2005, 2007a, 2010).

### 3.3. Edge feature extraction and matching

This section describes the edge extraction and matching methods. Fig. 3 outlines the steps for edge extraction and matching. Details for each step are described in the following sections.

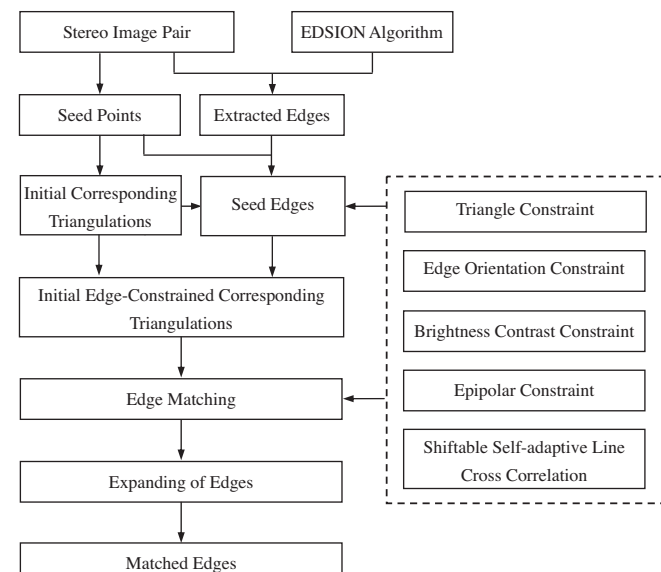


**Fig. 3.** Flowchart of edge feature extraction and matching.

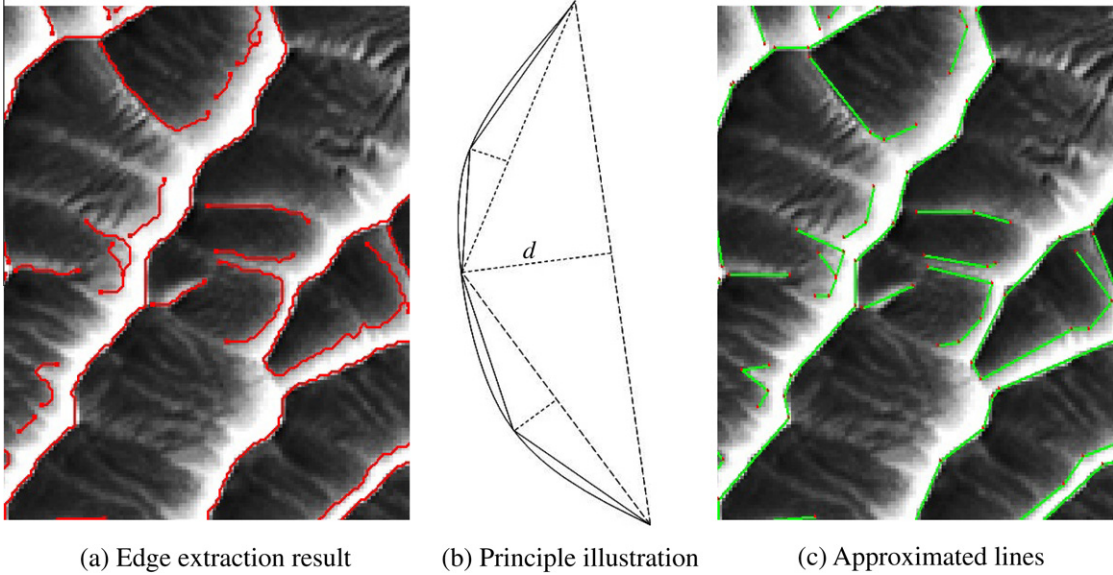


**Fig. 4.** Edge approximated to lines.

### 3.3.1. Edge feature extraction

A well-known edge extraction method, EDSION (Meer and Georgescu, 2001), is used to extract edge features from the stereo images. Fig. 4(a) shows a zoomed view of the extracted edges in the sand dune area on the HiRISE images of the Victoria crater on Mars (Fig. 1(a)). The extracted edges are then regularized to edge chains one-pixel wide. Before they can be used in the image matching, they need to be split and approximated to short line segments. The following algorithm is employed for this purpose:

- (1) For an extracted edge, link its two end-points to obtain a line, and then calculate the maximum arc-to-chord deviation of the edge from the line. The arc-to-chord deviation is defined as the perpendicular distance of a point on the edge to the line ( $d$  in Fig. 4(b));
- (2) If  $d$  exceeds a pre-defined threshold, split the edge at that point, and replace the original line with two new lines as illustrated in Fig. 4(b). The threshold  $L(d)$  is defined by the following equation as recommended by Zhang (2005):

$$L_d = \begin{cases} 1.0 + \log_{1.0} d & d \geq 1.0 \\ 1.0 & \text{otherwise.} \end{cases} \quad (1)$$

- (3) Repeat the previous two steps recursively for each segment, until all the segments have arc-to-chord deviations small enough. Then use the split lines to approximate the extracted edges.

Fig. 4(c) shows the edge approximation results from Fig. 4(a). Comparing these two figures, it is obvious that the approximated lines can represent the actual terrain features.

### 3.3.2. Constraints for edge matching

In this method, the edge features are matched based on the following fundamental constraints.

#### (i) Triangle constraint

The triangle constraint for edge matching is based on the following assumption, that is to say, if a pair of edges is matched to be a pair of corresponding edges then they should lie within the corresponding triangles. For example, for a given edge  $l$  on the left

image as illustrated in Fig. 5(a), its middle point  $O$  will be firstly identified. The triangle that contains  $O$  will then be identified. Then, starting from this triangle, a triangle list that contains the edge  $l$  will be tracked by searching the adjacent triangles. After that, their corresponding triangles on the right image will be identified, and all the edges having intersections with these triangles on the right image will be selected as matching candidates for the edge  $l$  on the left image. As shown in Fig. 5(b), there are five edges ( $l_1, l_2, l_3, l_4$ , and  $l_5$ ) selected as matching candidates for the edge  $l$  on the left image. This triangle constraint is helpful to reduce the search area of finding candidate matches and to improve the matching performance.

#### (ii) Edge orientation constraint

For stereo images with general perspective changes (the viewpoints for the two images are not significantly different), the orientations of the corresponding edges in local areas should be relatively consistent. Therefore, a loose constraint based on the edge orientations is employed in this method. That is to say, if the orientation difference between the matching edge and the candidate is larger than a pre-defined threshold ( $30^\circ$  recommended in this paper based on experimental analysis using regular satellite, aerial, and terrestrial images), this candidate will be excluded. For example, edge  $l_5$  in Fig. 5(b) will be excluded from the matching candidates for the edge  $l$  in Fig. 5(a) by applying the edge

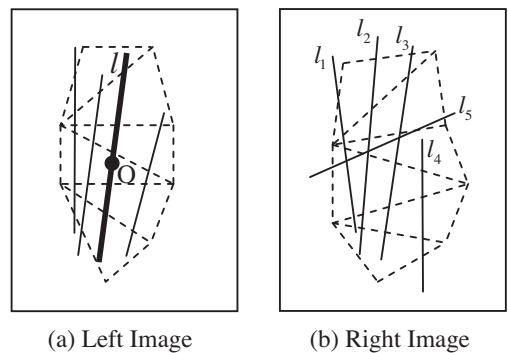


**Fig. 5.** Using triangle constraint to find matching candidates for edge matching.

orientation constraint. This edge orientation constraint can simply remove some obviously wrong candidates for edge matching.

### (iii) Brightness contrast constraint

Simple statistics of the brightness contrast in a local buffering region along both sides of the matching edges can be used to further disambiguate the edge matching. Assuming the equation expression for an edge is  $Ax + By + C = 0$ , for a local buffering region (11 pixels width used in this paper) centered at the edge, the average intensity on one side  $Ax + By + C < 0$  of the edge is  $I_1$ , and the average intensity for the other side  $Ax + By + C > 0$  of the edge is  $I_2$ . A brightness contrast attribute  $A_l$  for each edge is assigned as:

$$A_l = \begin{cases} -1 & I_1 - I_2 \geq 0 \\ 1 & \text{otherwise.} \end{cases} \quad (2)$$

Comparing the brightness contrast attributes of two matching edges, if they are equal then the two edges are considered as a possible match candidate, otherwise the candidate edge is excluded for further matching process.

### (iv) Epipolar constraint

If a pair of matching edges satisfies all the above constraints, then the epipolar constraint will be used to find out the corresponding overlap segments between the two edges. For example, for a pair of matching edges AC and BD in Fig. 6(a and b), the epipolar lines of the end points of AC and BD can be derived as illustrated using dashed lines in Fig. 6. By intersecting these epipolar lines with the edges AC and BD, the overlap segments between these two edges can be obtained, which is  $B'C$  and  $BC'$ .

Epipolar constraint works quite well for edges with large intersection angles with the epipolar lines. However, the intersection angles between the edges and the epipolar lines are sometimes small, which will bring ambiguities in determining the overlap segments. Especially when the edges to be matched are parallel to the epipolar lines, it is not possible to estimate the overlap segments between the edges. Therefore, this paper only uses this epipolar constraint to determine the overlap segments for the edges with intersection angles larger than a pre-defined threshold ( $30^\circ$  used in the paper based on experimental analysis using regular satellite, aerial, and terrestrial images) between them and the epipolar lines. For those edges with intersection angles less than the threshold, an edge to area matching strategy will be employed and details will be discussed in Section 3.4.2.

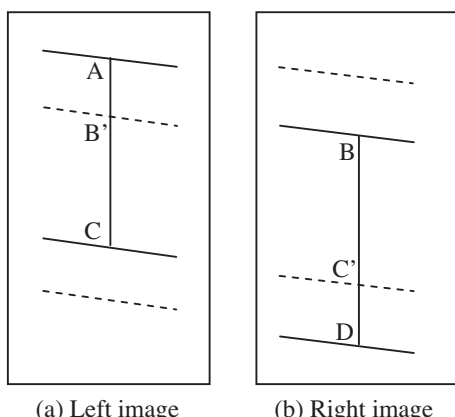


**Fig. 6.** Using epipolar constraint to find corresponding overlap segments for edge matching.

### 3.3.3. A Shiftable Self-adaptive Line Cross Correlation (SSLCC)

After edge matching candidates are selected and their overlap segments determined the next task is to measure the similarities between the edges to be matched. There have been several similarity descriptors presented for edge matching in the past decades, such as the Line Cross Correlation (LCC) based on the philosophy of Normalized Cross Correlation (NCC) for point matching (Schmid and Zisserman, 2000). LCC is determined by calculating the average of the NCCs for all the discrete pixels on the edges. Liu (2004) presented a Normalized Line Cross Correlation (NLCC) for edge matching, which uses a window with fixed size centered at the edges to calculate a window based NCC for the whole edge. Jiang (2004) developed a half-plane correlation method for edge matching, which only uses half of the window along one side of the edge to determine the correlation. This method is helpful to match the edges in occlusion textural areas where surface discontinuities may exist. However, it will reduce the distinctiveness of edge matching in other textural areas.

When using cross correlation to measure the similarity between the corresponding edges on the stereo images, the key issue is to select an appropriate window to calculate the correlations. The term "Appropriate" indicates the appropriate location, size, and shape of the correlation window. For interesting point matching, Kanade and Okutomi (1994) presented an adaptive cross-correlation method to select the appropriate correlation window size for image matching, which is an iterative process to extend the correlation window step by step toward the left, right, up, and down directions until the correlation values stop increasing. This method provides more accurate correlation windows and is ideal for point matching on images suffering from distortion or surface discontinuity problems. Bobick and Intille (1998) presented a cross-correlation method with a shiftable window to improve point matching performance on occlusion areas with surface discontinuity problems. Inspired from the discussed previous research, this paper presents a Shiftable Self-adaptive Line Cross Correlation (SSLCC) method for edge matching on poor textural images.

The SSLCC works in two steps. The first step is to use a shiftable window with fixed size (a width of 11 pixels used in this paper) to obtain an appropriate location for the correlation window. As illustrated in Fig. 7(a), for a pair of edges  $l$  and  $l'$  to be matched, a correlation window is moved starting from the left side of the edge to the right side along a direction perpendicular to the edge. A series of NLCC correlation values are calculated, and the window location with the highest correlation value is selected as the appropriate location of the correlation window. After the location of the correlation window is determined, the second step is to expand the window (with a step of 2 pixels) to the left or right side of the edge as illustrated in Fig. 7(b). The expansion will be stopped when the correlation values start to decrease. It should be noted that, if the window is just located on one side of the edge from the first step, then the window expansion is only needed in this side. After the window shift and expansion, the correlation value from the windows will be calculated, which is the SSLCC in this method. The value of SSLCC will range from  $-1$  to  $1$ . To determine whether a pair of edges is a potential match, the SSLCC should be larger than a pre-defined threshold. A higher threshold can lead to more accurate results but the numbers of the matched results will be less. Taking into account of the balance between the matched numbers and the matching accuracy, a threshold of 0.8 is used in the experiments reported in this paper.

### 3.3.4. Expanding of matched edges

For those matched edges which are not exactly the same length, which means one part of the edge extracted in one image is not successfully extracted in the other image, an edge expanding process is performed to obtain an edge pair with consistent lengths. As

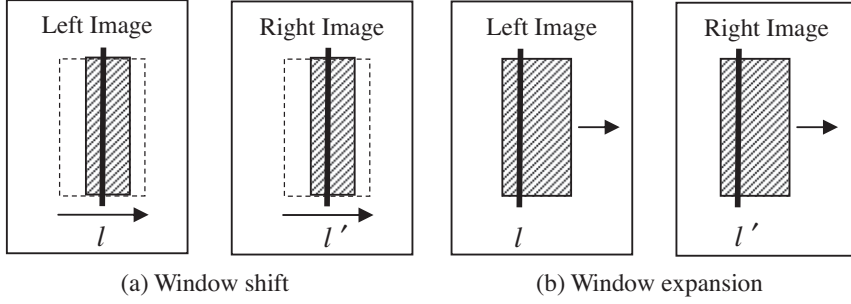


**Fig. 7.** Illustration of the Shiftable Self-adaptive Line Cross Correlation.

illustrated in Fig. 8(a), the overlap segments of two edges  $l$  ( $AC$ ) and  $l'$  ( $BD$ ) in a stereo pair is  $B'C$  and  $BC$ . They can be identified by the intersection of the edge and the epipolar line of the end point in the other edge. For segment  $AB'$  on edge  $l$  in the left image, its corresponding segment on edge  $l'$  in the right image is not successfully extracted. Similarly, segment  $CD$  on edge  $l'$  in the right image does not have its corresponding segment detected on edge  $l$  in the left image. The following edge expansion process is performed in both directions along with the edge pixel by pixel.

For the pixels beyond the overlap segments in the matching edges (e.g.,  $P$  on the segment  $AB'$  of edge  $l$  in the left image), the edge expanding algorithm tries to find its corresponding pixels on the other image so that to extend the corresponding edge. The edge expanding procedure starts from the end pixels of the overlap segments (e.g.,  $B'$  for the segment  $AB'$ ) and moves towards the end of the edge (e.g.,  $A$  for the edge  $AC$ ) pixel by pixel. As illustrated in Fig. 8(a), for a pixel  $P$  on segment  $AB'$  of edge  $l$  in the left image, its corresponding epipolar line  $e$  on the right image can be derived. The intersection point of the epipolar line  $e$  and the edge  $l'$  in the right image is  $P'$ , which is supposed to be the corresponding point of  $P$ . The NCC value between  $P$  and  $P'$  is calculated, and if the value is larger than a pre-defined threshold (e.g., 0.8), the matching

is accepted and the edge matching is expanded to  $P$  and  $P'$ ; otherwise, the edge expansion process is stopped. Edge expansion in another direction is performed in the same way.

Fig. 8(b) shows a zoomed view of the edges extracted along the rim of Victoria crater in the HiRISE images. As can be seen, the extracted edges do not overlapped ideally. The symbols of the end points on the edges show the same meaning as the symbols in Fig. 8(a). Fig. 8(c) is the matching results based on the matching constraints and SSLCC. As can be seen from Fig. 8(c), only the overlap segments have been matched. After the edge expansion process, the matched edges have been extended as shown in Fig. 8(d), and they are visually accurate.

### 3.3.5. Seed edge matching

Before the integrated point and edge matching propagation, a few seed edges are matched based on the seed points already obtained previously. The seed edge matching uses the prior information from the seed points and uses the triangle constraint, edge orientation constraint, brightness contrast constraint, and epipolar constraint. It should be noted that, the edges with intersection angles less than  $30^\circ$  between them and the epipolar lines are

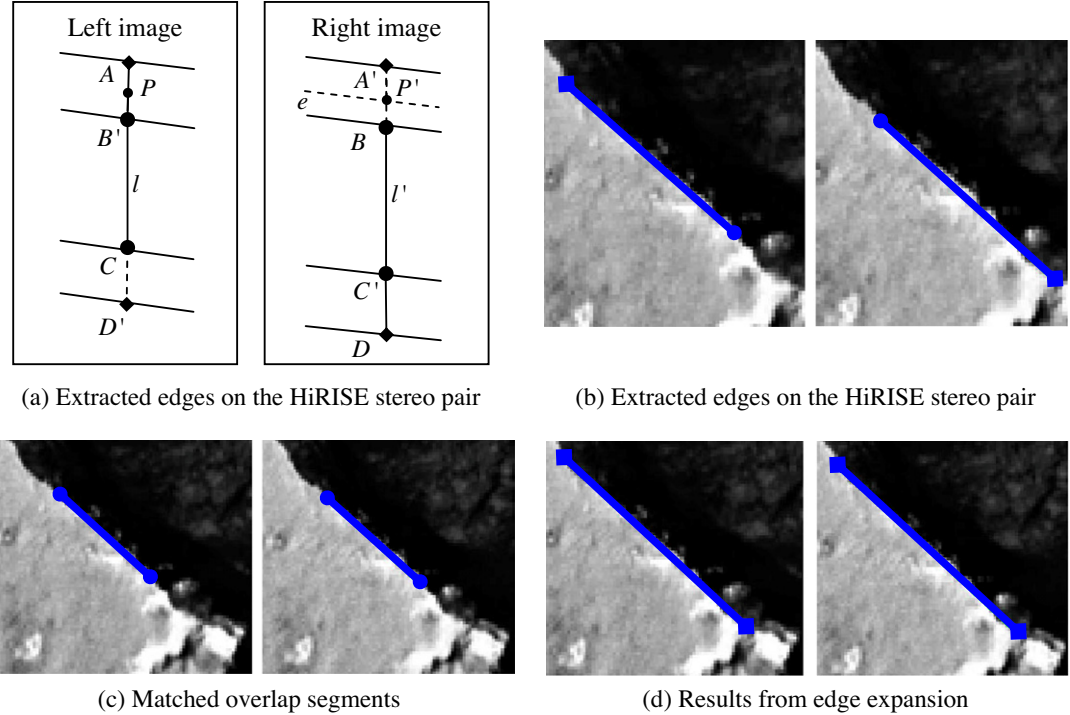


**Fig. 8.** Illustration of edge expansion.

excluded for seed edge matching. The seed edge matching algorithm works as in the following steps:

- (1) Select a seed point from the seed list and pick out several edges close to the selected seed point as seed edge candidates on the stereo images;
- (2) For each edge selected in the previous step in the left image, select the corresponding edges in the right image as matching candidates based on the triangle constraint, and then use the edge orientation constraint and brightness contrast constraint to exclude wrong candidates;
- (3) For the remaining candidates, use the epipolar constraint to obtain the overlap segments for each pair of the matches;
- (4) Calculate the SSLCC for every pair of the matches, and choose the one with maximum SSLCC and the SSLCC also larger than 0.8 as the matching hypothesis;

- (5) Carry out a “right to left” matching consistency check, if the bidirectional matching result is consistent, then the matching hypothesis is accepted as a successful match and edge expansion is employed, otherwise, reject the matching hypothesis;
- (6) Turn to step 2 to process the next unmatched edge until all the selected edges associated with that seed point are processed;
- (7) Turn to step 1 to process the next seed point until all the seed points are processed.

After a few seed edges are matched, all the seed edges and seed points are together used to generate a pair of initial edge-constrained Delaunay triangulations, which will be used to support the subsequent point and edge matching propagation.

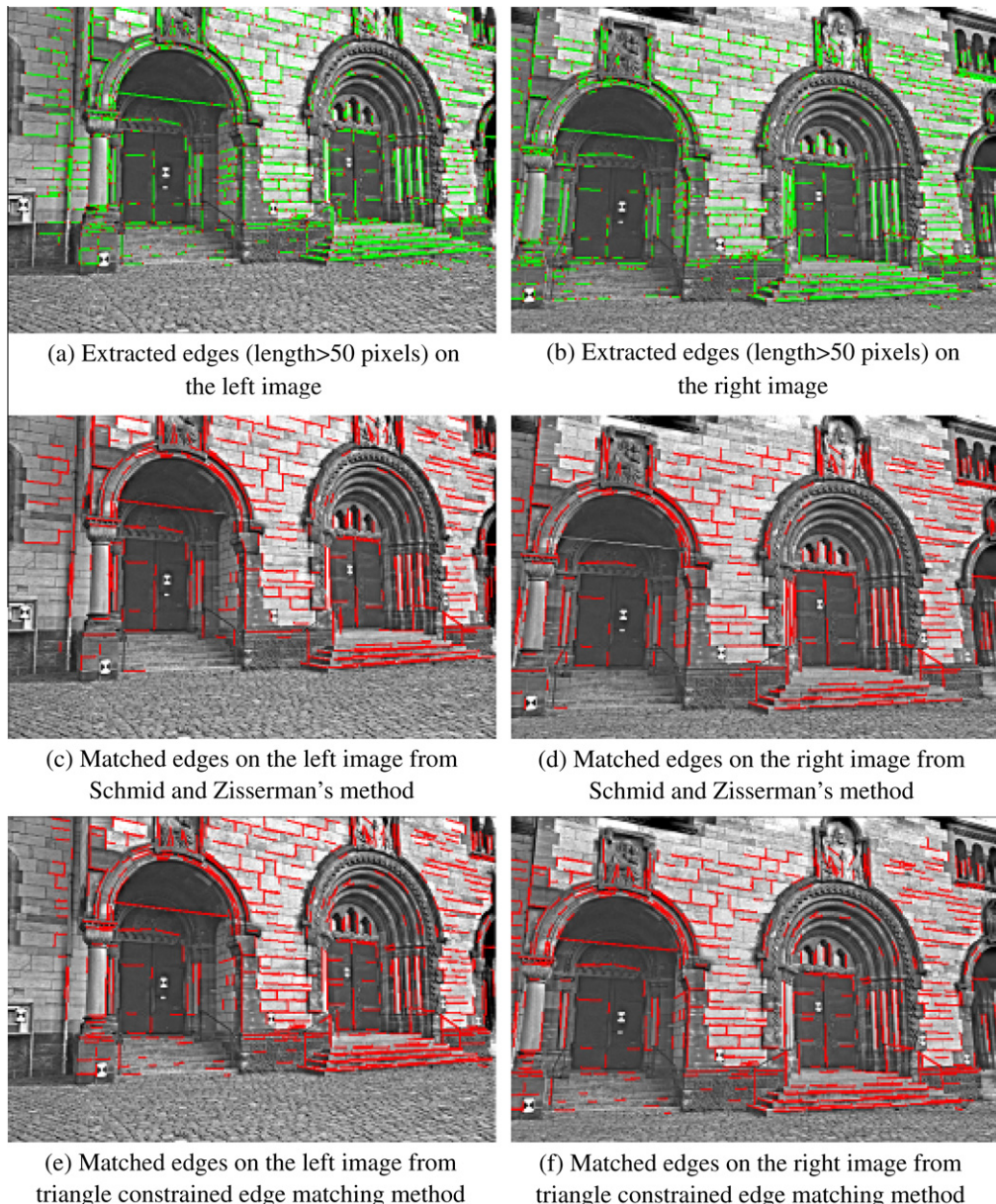


**Fig. 9.** Examples of stereo images with poor textures for image matching.

### 3.3.6. Evaluation of the triangle constrained edge matching method

To examine the performance of the triangle constrained edge matching method, the third stereo pair in Fig. 1 is used for experimental analysis since there are plenty of edges with regular shapes available on the images as can be seen in Fig. 1(e and f). Another classical edge matching method presented by Schmid and Zisserman (2000) is employed for comparison analysis. Schmid and Zisserman's method matches edges based on the epipolar constraint and the Line Cross Correlation (LCC). For the triangle constrained edge matching method, a pair of triangulations constructed from 23 seed points is used to constrain the edge matching. Point matching is not included in this experiment for comparison analysis. The results are shown in Fig. 9.

The EDSION algorithm is used to extract edges on the stereo images. Only those edges with lengths larger than 50 pixels are used for better experimental analysis. 722 edges on the left image and 781 edges on the right image are finally used and they are shown in Fig. 9(a and b), respectively. Using Schmid and Zisserman's method, 465 edges are matched as shown in Fig. 9(c and d), in which correct matches are 314 based on a manual check process. This indicates a matching accuracy of 67.5%. Fig. 9(d and f) show the matching results from the triangle constrained edge matching method presented in this paper. There are 588 edges matched and 580 are correct matches after manual checking, which indicates a matching accuracy of 98.6%. The eight mismatches mainly happened in the large triangles. By incorporating point matching in an integrated point and edge matching process, the triangulations will be quickly densified along with the matching propagation, which will provide stronger constraints for edge matching and further improve the edge matching accuracy. Details about the integrated point and edge matching propagation are discussed in the next section.

### 3.4. Integrated point and edge matching propagation

In image matching, the matching primitives with the most distinctiveness are usually the easiest to be matched and the matching is usually also reliable (Zhu et al., 2007b). On poor textural images, the distinctive features (either feature points or edges) are especially important and valuable for image matching. This triangulation based matching method exploits the prior information from these features by constructing triangulations based on them, and then use the triangulations to constrain the image matching. In this method, image matching always occurs in the areas with good textural conditions first, and then propagates the matching to the other poor textural areas by densifying the triangulations. The feature strength associated with the triangles and feature points or edges are employed to manipulate the matching propagation.

Feature strength (FS) is defined based on the distinctiveness of the features. For point features the Harris–Laplace interest strengths (Harris and Stephens, 1988; Zhu et al., 2007b) calculated through the response formulation in the point detecting process are used as FS. For edge features, the long edges are considered to be more distinctive than the short ones, and intuitively matching on long edges is supposed to be more stable than matching on short ones. Therefore, this paper uses the length of the edges to represent their distinctiveness. In order to manage the point and edge matching in an integrated structure, the length of the edges are normalized to a range between the maximum strength and minimum strength of the point features through a linear method. The normalized lengths are used as the FS for the edges, which are comparable to the FS of the point features. In addition to the point and edges, each triangle in the triangulations has also been assigned a FS, which is the average of the FS of its three vertices.

The integrated point and edge matching propagation starts from the initial edge-constrained triangulations generated from

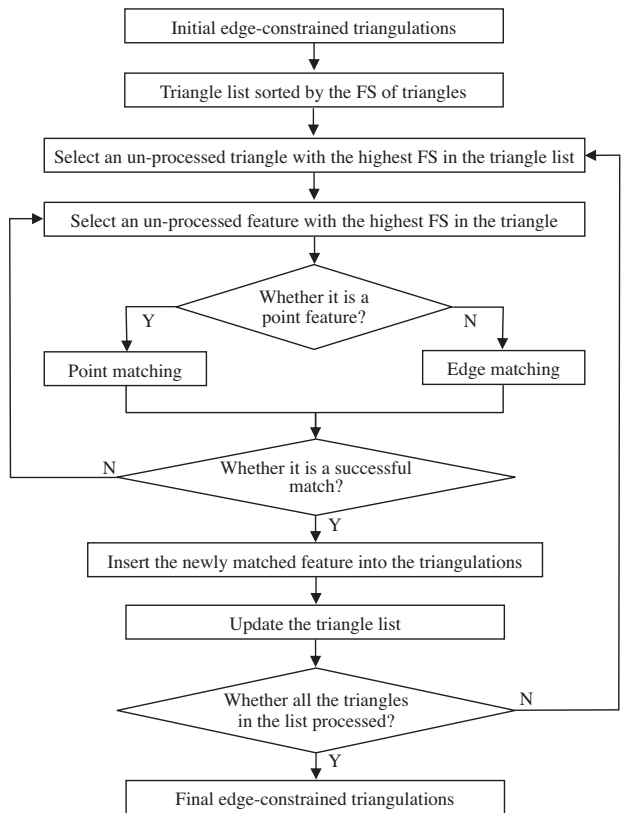


**Fig. 10.** Flowchart of the integrated point and edge matching propagation algorithm.

the seed points and edges. It follows the basic principles of the self-adaptive matching propagation strategy for interesting point matching as presented in Zhu et al. (2007a), but combines the edge matching in the matching propagation process and incorporates a “feature to area” matching process after the “feature to feature” matching. The flowchart of the integrated point and edge matching propagation algorithm is illustrated in Fig. 10, and the details of the “feature to feature” and “feature to area” matching process are described in the following sections.

#### 3.4.1. Feature to feature matching propagation

The feature to feature matching propagation includes both feature point and edge matching on both the stereo images. For edge matching, if the middle point of an edge is located within a triangle, then this edge is considered to be inside this specific triangle. The feature to feature matching propagation is described in Fig. 10. It mainly includes the following steps:

- (1) Select the left image as the reference image and the right image as the searching image. Calculate the FS for each triangle in the initial triangulations, and generate a triangle list by sorting the FS of the triangles on the reference image;
- (2) Select a triangle from the triangle list with the highest FS to process if it has not been processed yet, and obtain all the feature points and edges inside the triangle;
- (3) Select an unmatched feature with the highest FS inside the triangle; if it is a point feature, then go to step 4; if it is an edge feature, then go to step 5;
- (4) Match the point feature under the constraint of triangulations (Zhu et al., 2007a), if it is a successful matching, then go to step 6; otherwise go to step 3;

- (5) For the edge to be matched in the reference image, use the triangle constraint, edge orientation constraint, and brightness contrast constraint to exclude wrong candidates in the searching image. For the remaining candidates, use the epipolar constraint to obtain the overlap segments for each pair of the matches. Then, calculate the SSLCC for every pair of the matches, and choose the one with maximum SSLCC and the SSLCC also larger than a predefined threshold (e.g., 0.8) as the matching hypothesis. After that, carry out a “right to left” matching consistency check, if the bidirectional matching result is consistent, the matching hypothesis is accepted and an edge expansion process is employed, then go to step 6; otherwise, the matching hypothesis is rejected and go to step 3;
- (6) Insert the newly matched point or edge into the triangulations and update the triangle list, then turn to sept 2;
- (7) If all the triangles are processed, the matching propagation is terminated.

In this feature to feature matching propagation process, the most significant feature points and edges will be matched first. Along with the matching propagation, the image will be segmented into smaller local regions by the previous matched points and edges, and the remaining feature points and edges with less significance in the separated local regions can then be matched with less difficulty. It should be noted that, only those edges with intersection angles larger than  $30^\circ$  between them and the epipolar lines will be processed in this feature to feature matching propagation step. The rest of the edges will be processed in the later feature to area matching propagation step.

#### 3.4.2. Feature to area matching propagation

Due to the textural differences on the stereo images and the limitations of the feature detection methods, for the features detected in one image, not all their corresponding features can be detected in the other image. Also for edge matching particularly, those edges with intersection angles less than  $30^\circ$  between them and the epipolar lines are not considered in the previous steps. Therefore, this paper introduces a feature to area matching process

to take care of the matching of the rest of the features that have not been successfully matched before. The major steps of feature to area matching propagation are similar to those described in Fig. 10, except that the matching has been changed from “point to point” and “edge to edge” to “point to area” and “edge to area”, respectively.

Feature to area matching propagation starts from the edge-constrained triangulations derived from the previous feature to feature matching results. The image with more remaining features will be selected as the reference image, and the other one will be the searching image. For a given point in the reference image, all the pixels along the epipolar line inside the corresponding triangle in the searching image are treated as matching candidates. For all the candidates, matching scores are calculated and a score curve is then obtained. If the ratio of the highest matching score to the second highest matching score is larger than a predefined threshold (e.g., 1.25) and the highest matching score is larger than a threshold (e.g., 0.8), the correspondence is considered to be a matching hypothesis. If the hypothesis passes the double-direction consistency check, the correspondence is accepted as a correct match. Since the triangulations used here are already dense, they provide strong constraints to the point to area matching. Details about point to area matching based on the self-adaptive triangulations can be found in Wu et al. (2011).

For the remaining edges on the reference image, an edge to area matching method is developed as follows. First, the edge is divided into individual pixels. Then all the discrete pixels on the edge are treated as points, and their corresponding points in the searching image are obtained using the same method of point to area matching. After that, a RANSAC approach is employed to exclude possible mismatches and fit a new edge in the searching image. The RANSAC approach used here is based on the following assumption. For all the pixels on the edge, their disparities should satisfy a linear relationship to each other. The disparities of the pixels on an edge can be modeled by a linear function, which is used to build the model in the RANSAC approach. After the RANSAC process, the mismatches are removed, and the remaining matched pixels are fitted to an edge. If the fitted edge passes the edge orientation constraint and the brightness contrast constraint, and their SSLCC

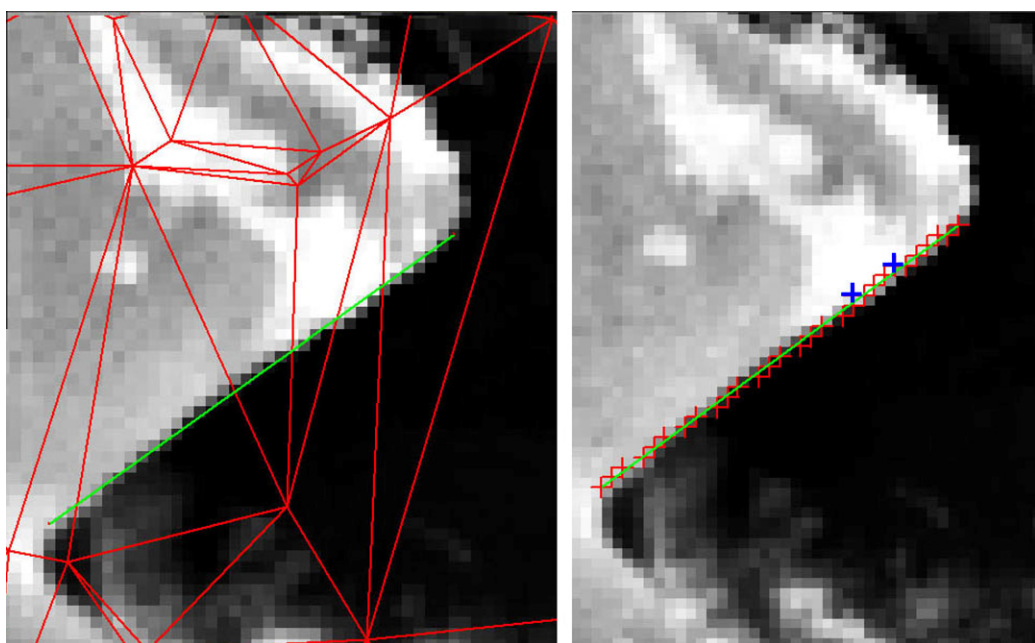


**Fig. 11.** Illustration of edge to area matching in the HiRISE stereo pair.

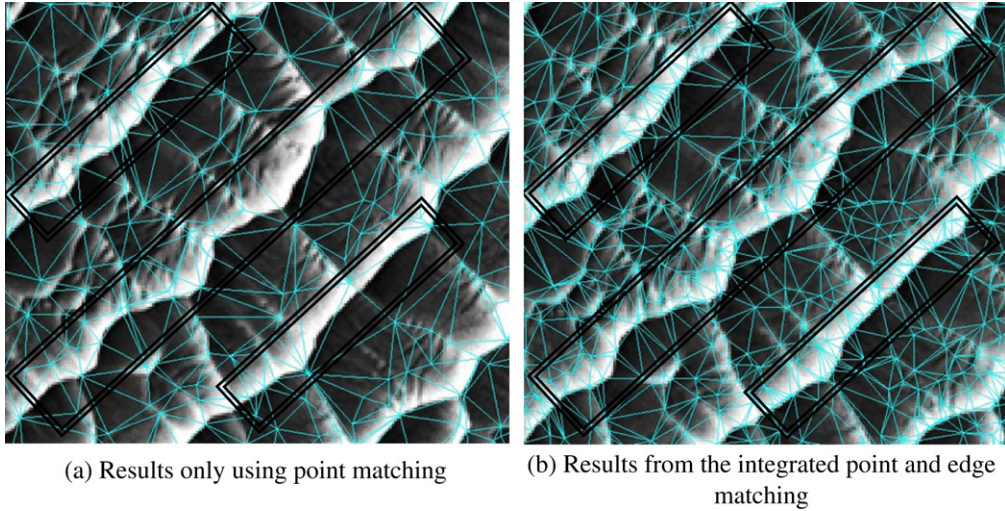


**Fig. 12.** Final triangulations from different matching strategy in the sand dune area of Victoria crater on the HiRISE image.

is larger than 0.8, then the fitted edge is accepted as a correct match.

**Fig. 11** shows an example of edge to area matching along the rim of Victoria crater in the HiRISE stereo pair. The edge extracted in the left image has an intersection angle less than 30° with the epipolar line. After matching the individual pixels on the edge to the right image, 36 matched pixels have been obtained as shown as crosses in **Fig. 11**, in which two of them labeled with thick blue are classified as outliers after the RANSAC process. Then all the remaining matched pixels are fitted to an edge, which turns out to finally be the correct match of the edge in the left image.

After the integrated point and edge matching propagation, the output is the final edge-constrained triangulation. **Fig. 12** shows examples in the sand dune area of Victoria crater on the HiRISE images. **Fig. 12(a)** is the result only using points as matching primitives also based on the self-adaptive triangle constraint ([Zhu et al., 2007a](#)) named as “point matching”. The other is the traditional image matching method based on the Normalized Cross Correlation ([Lhuillier and Quan, 2002](#)) under the epipolar constraint named as “NCC”.

constraint (named as “integrated point and edge matching”) are compared with the results from the other two methods. One is the method only using points as matching primitives also based on the self-adaptive triangle constraint ([Zhu et al., 2007a](#)) named as “point matching”. The other is the traditional image matching method based on the Normalized Cross Correlation ([Lhuillier and Quan, 2002](#)) under the epipolar constraint named as “NCC”.

In order to quantitatively evaluate the performance of the image matching methods, the 3D coordinates of the matched results are calculated based on the image internal orientation (IO) and external orientation (EO) parameters. They are then compared with certain reference data (e.g., digital elevation data derived from digital photogrammetric systems or laser scanning, or randomly selected checkpoints with known coordinates). Their height differences are computed and their statistics of RMSE (root mean squared error) and maximum values are obtained, which are used as indicators of the performance of image matching.

#### 4.1. Experiments using the HiRISE stereo pair

The integrated point and edge matching method, the point matching method, and the NCC method have been used to process the HiRISE stereo images as illustrated in **Fig. 1(a and b)**. The basic matching criteria for these three methods are set to be the same, for example, the thresholds of the cross-correlation coefficients to be considered as a potential match are 0.8 for all the three methods, and the termination conditions of the triangle constrained

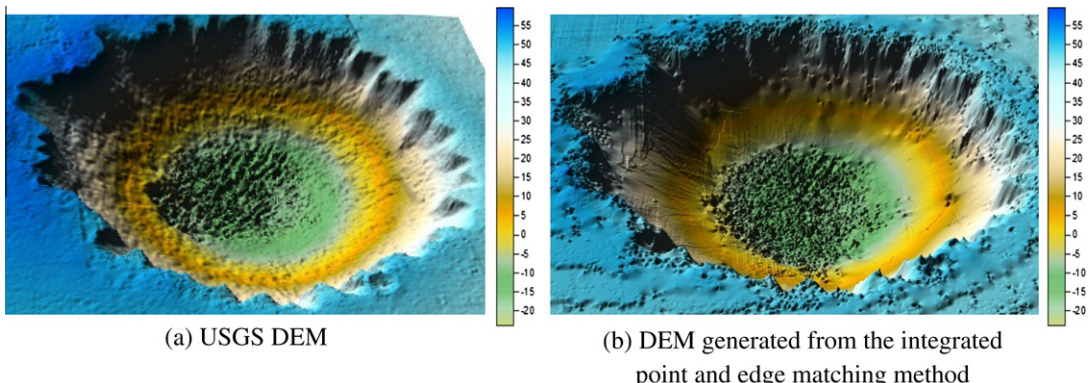


**Fig. 13.** DEM comparison.

matching propagation for the previous two methods are the same. Finally, three sets of matching results are obtained, and they are used in the subsequent quantitative comparison.

The US Geological Survey (USGS) has processed the HiRISE stereo pair at Victoria crater on Mars using their in-house digital cartographic software ISIS and the commercial photogrammetric software SOCET SET for DEM production (Kirk et al., 2007). Kirk et al. (2007) also mentioned that intensive interactive editing was performed to produce a 1 m resolution DEM when using the software systems due to the extremely unfavorable image textural conditions. The DEM was downloaded from the Mars HiRISE DEM archives in NASA's Planetary Data System (PDS) (<http://hirise.lpl.arizona.edu/dtm/>, accessed on November 11, 2010) and is illustrated in Fig. 13(a). It has been used as a reference for comparison analysis in this paper.

Thirty two control points (feature points) are manually identified from the HiRISE stereo images. Their 3D coordinates are also obtained from the DEM generated by USGS. These control points are evenly distributed in the crater rim, wall, and bottom areas. They are used to build a transformation relationship between the image space and the object space using the 3D DLT (Direct Linear Transformation) method (Hatzes, 1988), in which eight control points are used to calculate the initial 16 DLT parameters (including 11 standard DLT parameters and five optical distortion terms) and the rest of the control points are used to refine the parameters through a least-square approach. Using the calculated DLT parameters, the 3D coordinates of the matched points/edges from the three matching methods are obtained, from which DEMs with 1 m resolutions are interpolated. Fig. 13(b) shows the 3D view of the DEM directly derived from the integrated point and edge matching method without any manual editing.

From Fig. 13, it can be seen that the topography derived from the integrated point and edge matching method is consistent with the USGS DEM in general. To quantitatively evaluate the image matching results, all the derived 3D points (including the start and end pixels for the matched edges) from the three matching methods are used as check points and their elevations are compared to the corresponding elevation values directly interpolated from the USGS DEM. The RMSE and maximum value of the eleva-

tion difference are calculated as indicators of the performance of image matching. The detailed comparison results are listed in Table 1.

From Table 1, it can be seen that the integrated point and edge matching method produces the best results. Comparing the RMSE results of the three methods, NCC produces the largest RMSE of 17.16 m, which may be caused by the possible mistakes in the image matching on the poor textural images. While the RMSE results for the other two methods are significantly improved. The RMSE from the integrated point and edge matching method is better than the RMSE from the point matching method, and the number of the successfully matched points significantly increased from 11,920 to 40,657 after incorporating the edge matching. In addition 1533 edges have been successfully matched.

To have a detailed comparison analysis, three difference DEMs are derived by subtracting the USGS DEM from the DEMs generated from the three image matching methods. They are shown in Fig. 14. It should be noted that different color scales are used for the difference DEMs. Statistics including maximum and minimum differences, and the mean as well as the standard deviation of the differences are calculated. For the difference DEM derived from the NCC method, the maximum, minimum, mean, and standard deviation of the differences are 192.13 m, -393.35 m, -2.45 m, and 6.97 m, respectively. For the difference DEM derived from the point matching method, the maximum, minimum, mean, and standard deviation of the differences are 11.20 m, -17.07 m, -2.84 m, and 2.60 m, respectively. For the difference DEM derived from the integrated point and edge matching method, the maximum, minimum, mean, and standard deviation of the differences are 7.60 m, -17.04 m, -2.12 m, and 2.48 m, respectively. The statistics show that the integrated point and edge matching method produces the best results.

#### 4.2. Experiment using the aerial stereo pair in highland area in Lanzhou, China

The aerial stereo images acquired in the highland area in Lanzhou, China as shown in Fig. 1(c and d) have also been used in experimental analysis. Fig. 15 shows the image matching results.

There are 6297 and 6396 edges extracted from the left image and right image of the aerial stereo images, respectively. And finally, 4999 edges are successfully matched from the integrated point and edge matching method, which are shown in Fig. 15(a and b). From Fig. 15(a and b), it is encouraging that the matched edges can generally represent the layer structure of the highland area. Fig. 15(c and d) is the zoomed view of a local region as marked with rectangles in Fig. 15(a and b) showing the final triangulations from point matching and integrated point and edge matching, respectively. It can be found that, if only using point matching,

**Table 1**  
Experimental result using the HiRISE stereo pair.

Image matching method	Number of matched points or edges	Maximum difference (m)	RMSE (m)
NCC	Points: 18,189	281.59	17.16
Point matching	Points: 11,920	29.80	1.27
Integrated point and edge matching	Points: 40,657; edges: 1533	29.14	0.99

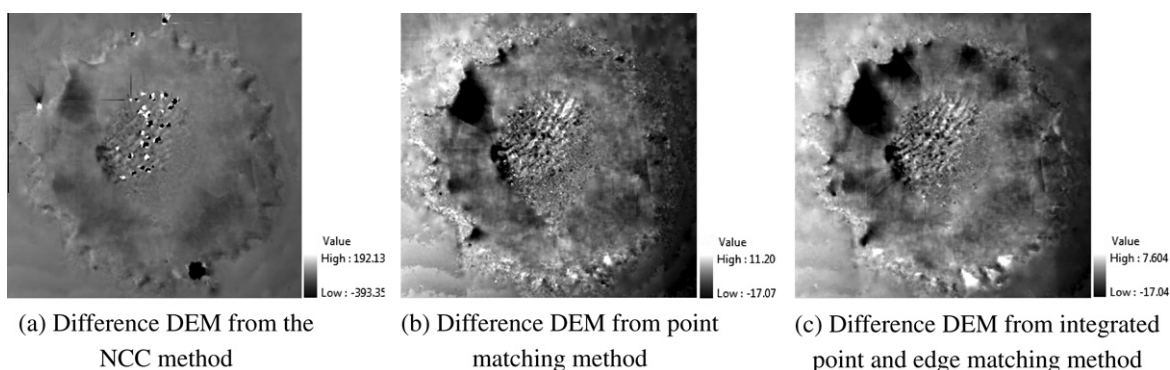


**Fig. 14.** Differences between the USGS DEM and the DEMs generated from the different image matching methods.

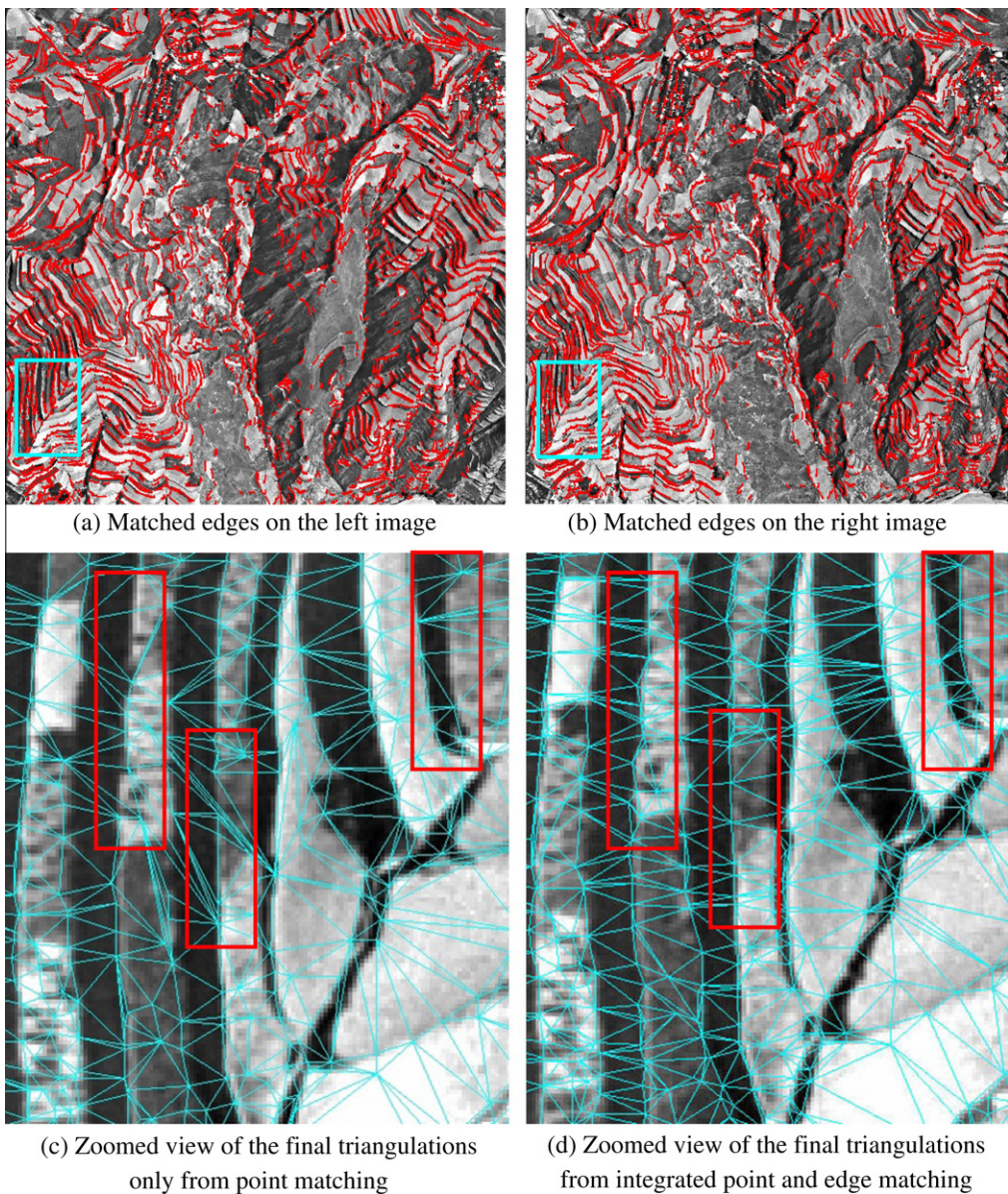


**Fig. 15.** Matching results from the aerial stereo images acquired in the highland area in Lanzhou, China.

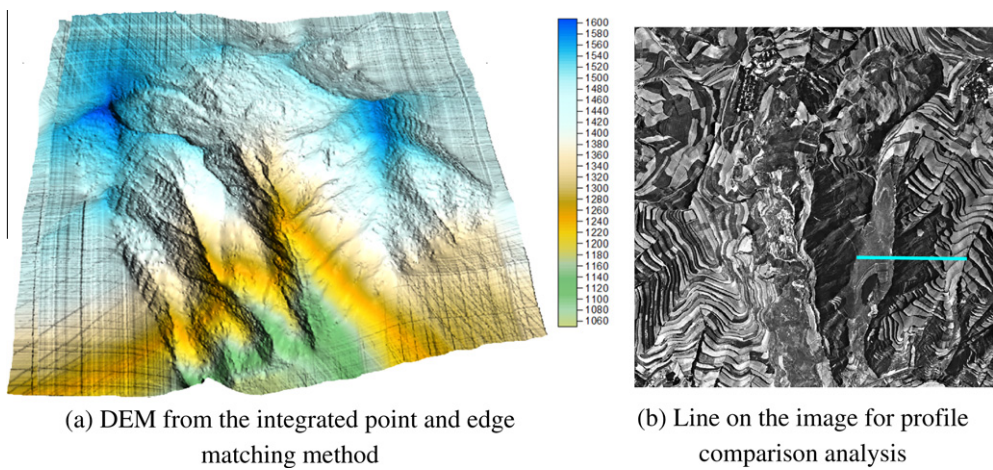


**Fig. 16.** Generated DEM and the line used for profile comparison analysis.

**Table 2**

Experimental result using the aerial stereo pair.

Image matching method	Number of matched points or edges	Maximum difference (m)	RMSE (m)
NCC	Points: 21,607	49.43	14.73
Point matching	Points: 25,646	13.84	3.09
Integrated point and edge matching	Points: 68,061; edges: 4999	9.43	2.20

some edge features cannot be successfully matched and the final triangles may cross edges which they should not, such as those regions marked with rectangles in Fig. 15(c and d).

To quantitatively evaluate the performances of the three image matching methods, three DEMs are generated using the matched results from the three methods, respectively. The image internal orientation (IO) and external orientation (EO) parameters are provided for DEM generation. Fig. 16(a) shows the DEM generated from the integrated point and edge matching results. Since no ground truth data is available for this study area, 268 points are manually measured by using a commercial photogrammetric software system, VirtuoZo Digital Photogrammetry Workstation. They are evenly distributed in the image area. They are used as check points and their elevations are compared to the corresponding elevation values directly interpolated from the DEM. The detailed comparison results are listed in Table 2. From Table 2, it can be seen that the integrated point and edge matching method produces the best results. Similar trends with the previous experiments using the HiRISE stereo images can be found for the RMSE results and the numbers of the successfully matched points or edges. It should be noted that the relatively large RMSE results in

this experiment may be caused by the possible systematic errors in the manually identified check points when using the commercial software. But this does not affect the overall assessment of the three image matching methods.

To better understand the performance of different image matching methods using this data set, a line is drawn in the image which covers the regions with significant elevation variations as shown in Fig. 16(b). Referring to this line different profiles are derived as shown in Fig. 17, in which the red solid line represents the profile directly measured from the VirtuoZo Workstation, the red dash line indicates the profile derived from the DEM interpolated from the matched results of the integrated point and edge matching method, the solid blue line is derived from the DEM based on the point matching results, and the dash blue line is obtained from the DEM based on the matched results of the NCC method. From the profiles, it can be noticed that the one derived from the

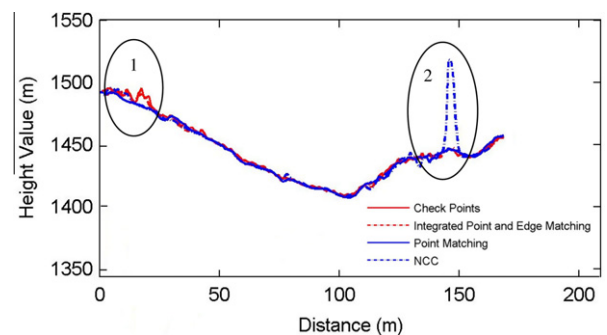


Fig. 17. Profile comparison of the image matching methods.

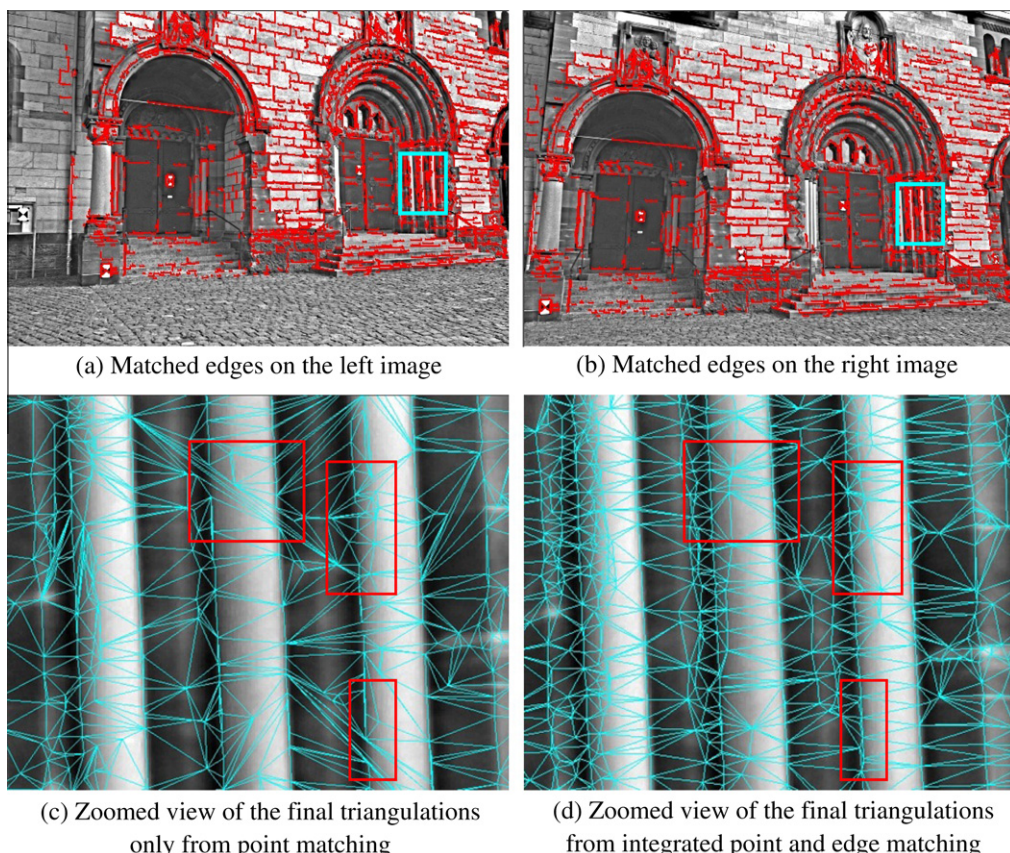
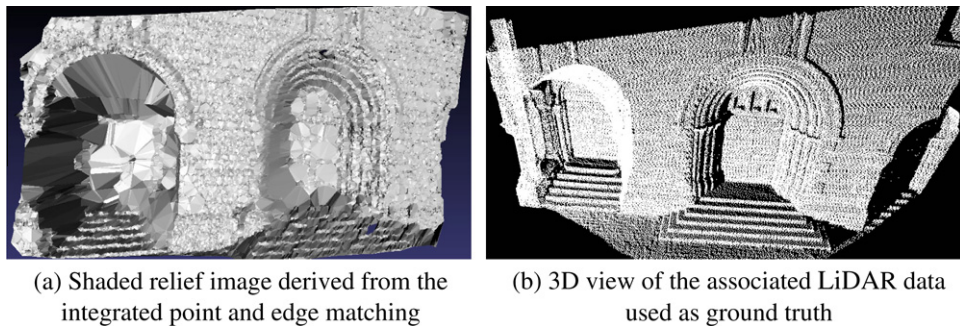


Fig. 18. Matching results from the stereo terrestrial images.



**Fig. 19.** Generated shaded relief image and the associated LiDAR data for the experiments using the stereo terrestrial images.

**Table 3**  
Experimental result using the aerial stereo pair.

Image matching method	Number of matched points or edges	Maximum difference (m)	RMSE (m)
NCC	Points: 21,494	18.56	1.89
Point matching	Points: 11,392	12.87	0.35
Integrated point and edge matching	Points: 51,246; edges: 2919	12.86	0.31

integrated point and edge matching method is closest to the profile directly measured from the VirtuoZo Workstation. In the area labeled as 1, only the profile from the integrated point and edge matching method shows reasonable results. For the area labeled as 2, the profile from NCC shows obvious errors.

#### 4.3. Experiment using the stereo pair of terrestrial building images

The stereo terrestrial images shown in Fig. 1(e and f) were downloaded from the Computer Vision Laboratory of EPFL in Switzerland (Strecha et al., 2008) (<http://cvlab.epfl.ch/~strecha/multi-view/denseMVS.html>), accessed on December 11, 2010). The image IO and EO parameters are provided, and the downloaded data sets also include the LiDAR point cloud data associated with the image scene which will be used as ground truth in the experimental analysis. Fig. 18 shows the image matching results.

There are 7676 and 6765 edges extracted from the left image and right image of the stereo terrestrial images, respectively. And finally, 2919 edges are successfully matched from the integrated point and edge matching method, which are shown in Fig. 18(a and b). From Fig. 18(a and b), it can be seen that the matched edges cover almost all the inter-edges of the brick structure of the building wall. Fig. 18(c and d) is the zoomed view of a local region as marked with rectangles in Fig. 18(a and b) showing the final triangulations from point matching and integrated point and edge matching, respectively. It can be found that, if only using point matching, some triangles have anomalous shapes that may be caused by mistakes in the point matching and some edge features cannot be successfully matched, such as those regions marked with rectangles in Fig. 18(c and d).

To quantitatively evaluate the performances of the three image matching methods, 3D points are derived based on the matching results using the provided image IO and EO parameters. Fig. 19(a) shows the shaded relief image of the 3D points derived from the integrated point and edge matching results. The downloaded LiDAR point cloud data is illustrated in Fig. 19(b). The LiDAR data are well aligned with the images already so that it can be used as ground truth for comparison analysis (Strecha et al., 2008). To compare the 3D points derived from the stereo images with the LiDAR data, the LiDAR points are firstly back-projected onto the image pairs using the IO and EO parameters of the images, and those LiDAR points whose back-projected points overlapped with the

matched points from the stereo images are selected as check points for further comparison. The overlap areas cover all the matched results for the three image matching methods. The detailed comparison results are listed in Table 3.

From Table 3, it can be seen that the experimental results are consistent with the results from previous experiments. The integrated point and edge matching method produces the best results. Similar trends with previous experiments can be found for the RMSE results and the numbers of the successfully matched points or edges.

## 5. Conclusions and discussion

This paper presented a feature-preserving image matching method for reliable image matching on poor textural images by integrating point and edge matching in the same matching propagation process based on the self-adaptive edge-constrained triangulations. The experiment analyses using typical space-borne, airborne, and terrestrial images with poor textures conveyed the following conclusions:

- (1) Edge matching is very valuable for image matching on poor textural images since the edge matching process is also an image segmentation process, which is helpful to reduce matching ambiguity in poor textural conditions;
- (2) In the integrated point and edge matching method, edge matching, and point matching are performed in the same matching propagation process based on the edge-constrained triangulations, in which the real-time results from edge matching are used to support the point matching and vice versa. As a result, dense and reliable matching results can be obtained, which is hard to achieve when only using point matching method;
- (3) From the final matched points and edges, 3D points and edges preserving the physical boundaries of objects can be further derived based on photogrammetric techniques. They are ideal data sets for further object modeling applications.

It is very valuable to exploit the available edge feature information to support reliable image matching, especially on images with poor textural conditions. The experimental results reported in this paper are promising. Future research will analyze the characteristics of different poor textural situations and use a texture measure to characterize the poor texture so that a better understanding of the performance of the developed method can be obtained under different textural conditions. Future efforts will also include the effectiveness of the developed method on other extremely difficult matching cases, such as matching on the images in metropolitan areas where tall buildings are densely located, which leads to severe occlusion problems. Tests over areas by a larger number of images are also of interest.

## Acknowledgement

The work described in this paper was supported by a Grant from the Research Grants Council of Hong Kong (Project No. PolyU 5312/10E), and Grants from the Start-up Research Fund Program (1-ZV6K) and the Internal Competitive Research Grant (A-PJ62) of the Hong Kong Polytechnic University. The research was also supported by the National Basic Research Program of China/973 Program (Project No. 2010CB731801), and National Natural Science Foundation of China (Project No. 41021061).

## References

- Bay, H., Ess, A., Tuytelaars, T., Van Gool, L., 2008. Speeded-Up Robust Features (SURF). *Computer Vision and Image Understanding* 110 (3), 346–359.
- Bobick, A.F., Intille, S.S., 1998. Large occlusion stereo. *International Journal of Computer Vision* 33 (3), 181–200.
- Fischler, M.A., Bolles, R.C., 1981. Random sample consensus: a paradigm for model fitting with application to image analysis and automated cartography. *Communications of the ACM* 24 (6), 381–395.
- Furukawa, Y., Ponce, J., 2010. Accurate, dense, and robust multiview stereopsis. *IEEE Transactions on Pattern Analysis and Machine Intelligence* 32 (8), 1362–1376.
- Harris, C., Stephens, M., 1988. A combined corner and edge detector. *Proceedings of fourth Alvey Vision Conference*, Manchester, pp. 147–151.
- Hartley, R., Zisserman, A., 2003. *Multiple View Geometry in Computer Vision*, second ed. Cambridge University Press, 672 pages.
- Hatze, H., 1988. High-precision three-dimensional photogrammetric calibration and object space reconstruction using a modified DLT approach. *Journal of Biomechanics* 21 (7), 533–538.
- Heipke, C., Oberst, J., Albertz, J., Attwenger, M., Dorninger, P., Dorrer, E., Ewe, M., et al., 2007. Evaluating planetary digital terrain models - The HRSC DTM test. *Planetary and Space Science* 55 (2007), 2173–2191.
- Jiang, W., 2004. Multiple aerial image matching and automatic building detection. Ph.D. Dissertation, Wuhan University, 143 pages.
- Kanade, T., Okutomi, M., 1994. A stereo matching algorithm with an adaptive window: theory and experiment. *IEEE Transactions on Pattern Analysis and Machine Intelligence* 16 (9), 920–932.
- Kirk, R.L., E. Howington-Kraus, M.R. Roseik, D. Cook, J. Anderson, K. Becker, B.A. Archinal, L. Keszthelyi, R. King, A.S. McEwen, and the HiRISE Team, 2007. Ultrahigh Resolution Topographic Mapping of Mars with HiRISE stereo images: methods and first results, *Proceedings Lunar Planet Science Conference* 38th, abstract 1428.
- Lhuillier, M., Quan, L., 2002. Match propagation for image-based modeling and rendering. *IEEE Transactions on Pattern Analysis and Machine Intelligence* 24 (8), 1140–1146.
- Liu, Y., 2004. A semi-automatic algorithm for line matching based on Delaunay triangulation. *Geomatics and Information Science of Wuhan University* 29 (4), 342–346.
- Lowe, D.G., 1999. Object recognition from local scale-invariant features. *International Conference on Computer Vision*, Corfu, Greece, pp. 1150–1157.
- Lowe, D.G., 2004. Distinctive image features from scale-invariant keypoints. *International Journal of Computer Vision* 60 (2), 91–110.
- Match-T DSM, 2011. [http://www.inpho.de/index.php?seite=index\\_match-t](http://www.inpho.de/index.php?seite=index_match-t). (Accessed on January 10, 2011).
- McEwen, A.S., Eliason, E.M., Bergstrom, J.W., Bridges, N.T., Hansen, C.J., Delamere, W.A., Grant, J.A., et al., 2007. Mars Reconnaissance Orbiter's High Resolution Imaging Science Experiment (HiRISE). *Journal of Geophysical Research-Planets* 112 (E05S02). doi:10.1029/2005JE002605.
- Meer, P., Georgescu, B., 2001. Edge detection with embedded confidence. *IEEE Transactions on Pattern Analysis and Machine Intelligence* 23 (12), 1351–1365.
- Mikolajczyk, K., Schmid, C., 2004. Scale & affine invariant interest point detectors. *International Journal of Computer Vision* 60 (1), 63–86.
- Otto, G.P., Chau, T.K., 1989. A region-growing algorithm for matching of terrain images. *Image and Vision Computing* 7 (2), 83–94.
- Schmid, C., Zisserman, A., 2000. The geometry and batching of lines and curves over multiple views. *International Journal of Computer Vision* 40 (3), 199–233.
- Seitz, S.M., Curless, B., Diebel, J., Scharstein, D., Szeliski, R., 2006. A comparison and evaluation of multi-view stereo reconstruction algorithms. *IEEE Computer Society Conference on Computer Vision and Pattern Recognition*, Washington, DC, US, pp. 519–528.
- Strecha, C., Hansen, W.V., Gool, L.V., Fua, P., Thoennessen, U., 2008. On benchmarking camera calibration and multi-view stereo for high resolution imagery. *IEEE Computer Society Conference on Computer Vision and Pattern Recognition*, Anchorage, AK, pp. 1–8.
- Tao, H., Sawhney, H.S., Kumar, R., 2001. A global matching framework for stereo computation. *International Conference Computer Vision*, Vancouver, British Columbia, Canada, pp. 532–539.
- Tola, E., Lepetit, V., Fua, P., 2010. DAISY: an efficient dense descriptor applied to wide-baseline stereo. *IEEE Transactions on Pattern Analysis and Machine Intelligence* 32 (5), 815–830.
- Wu, B., 2006. A Reliable Stereo Image Matching Method Based on the Self-adaptive Triangle Constraint, Ph.D. Dissertation, Wuhan University, China, pp. 110.
- Wu, B., Zhang, Y.S., Zhu, Q., 2011. A triangulation-based hierarchical image matching method for wide-baseline images. *Photogrammetric Engineering & Remote Sensing* 77 (7), 695–708.
- Zhang, L., 2005. Automatic digital surface model (DSM) generation from linear array images. Ph.D. Dissertation, Institute of Geodesy and Photogrammetry, Swiss Federal Institute of Technology Zurich, pp. 219.
- Zhang, C., Fraser, C.S., 2009. An improved approach for DSM generation from high-resolution satellite imagery. *Journal of Spatial Science* 54 (2), 1–13.
- Zhang, L., Gruen, A., 2006. Multi-image matching for DSM generation from IKONOS imagery. *ISPRS Journal of Photogrammetry and Remote Sensing* 60 (3), 195–211.
- Zhang, B., Miller, S., Walker, S., Devenecia, K., 2007. Next generation automatic terrain extraction using Microsoft ultracam imagery. *ASPRS 2007 Annual Conference*, Tampa, Florida, pp. 12 (on CD-ROM).
- Zhu, Q., Zhao, J., Lin, H., Gong, J.Y., 2005. Triangulation of well-defined points as a constraint for reliable image matching. *Photogrammetric Engineering & Remote Sensing* 71 (9), 1063–1069.
- Zhu, Q., Wu, B., Tian, Y., 2007a. Propagation strategies for stereo image matching based on the dynamic triangle constraint. *ISPRS Journal of Photogrammetry and Remote Sensing* 62 (4), 295–308.
- Zhu, Q., Wu, B., Wan, N., 2007b. A filtering strategy for interest point detecting to improve repeatability and information content. *Photogrammetric Engineering & Remote Sensing* 73 (5), 547–553.
- Zhu, Q., Zhang, Y., Wu, B., Zhang, Y., 2010. Multiple close-range image matching based on a self-adaptive triangle constraint. *Photogrammetric Record* 25 (132), 437–453.